An Open Source Conceptual Sizing Model for the Hyperloop Passenger Pod

Jeffrey C. Chin
Research Aerospace Engineer
NASA Glenn Research Center
Propulsion Systems Analysis Branch
Cleveland OH, 44135
Email: jeffrey.c.chin@nasa.gov

Justin S. Gray
Research Aerospace Engineer
NASA Glenn Research Center
Propulsion Systems Analysis Branch
Cleveland OH, 44135
Email: justin.s.gray@nasa.gov

Scott Jones
Senior Research Aerospace Engineer
Jeffrey Berton
Senior Research Aerospace Engineer
NASA Glenn Research Center
Propulsion Systems Analysis Branch
Cleveland OH, 44135

Hyperloop is a transportation concept proposed as a faster, cheaper alternative to California's high speed rail project. It consists of a passenger pod traveling through a tube under light vacuum, suspended on air bearings. The original proposal looks promising, but assumes tube and pod dimensions are independently sizable without fully acknowledging constraints on compressors and pod geometry. Using open-source toolsets a new sizing method is developed, focusing on the strong thermodynamic interactions between the tube and pod. These additional considerations require doubling the proposed tube diameter, limiting maximum pod speed to 620 mph, and increasing overall travel time by five minutes. In addition, the proposed on-board heat exchangers are unideal for achieving reasonable equilibrium tube temperatures. Removal of this subsystem would reduce pod weight, energy, and complexity. In light of these findings, the core concept remains compelling, although additional engineering and economic analyses are markedly necessary to quantify feasibility.

Nomenclature

β Volume coefficient of expansion
$\dot{m}$ Mass flow rate
ε Emissivity Factor
γ Heat Capacity Ratio
ρ Total, Hemispherical Reflectivity
σ Stefan-Boltzmann constant
υ Kinematic Viscosity
BF Blockage Factor, diffused area over pod area
c1MN Mach number,front face of the first compressor
C_p Heat capacity at constant pressure
c_{solar} Gross Irradiance Adjustment
G Solar Irradiance
g Acceleration due to gravity
Gr Grashof Number
h Heat transfer coefficient
k Thermal Conductivity
L Length
MN Mach Number
NTU Number of Transfer Units
NU Nusselt Number
P Pressure
L Length
Pr Prandtl Number
Q Heat flow rate
Ra Rayleigh Number
T Temperature
η_{ad} Adiabatic Efficiency

1 Introduction

Hyperloop is a conceptual transportation system designed to lower costs and travel times relative to California's current high-speed rail project. [**?**] Elon Musk and a team of engineers from Tesla Motors and the Space Exploration Technologies Corporation (SpaceX) proposed the idea in August 2013 as an open design to be vetted and further refined through public contribution. The concept deviates from existing high-speed rail designs by eliminating the rails, enclosing the passenger pod in a tube under a partial vacuum,

and suspending the pod on air bearings. Propulsion is handled by a set of linear electromagnetic accelerators mounted to the tube with the entire system held above ground on concrete columns maintaining a relatively straight trajectory.

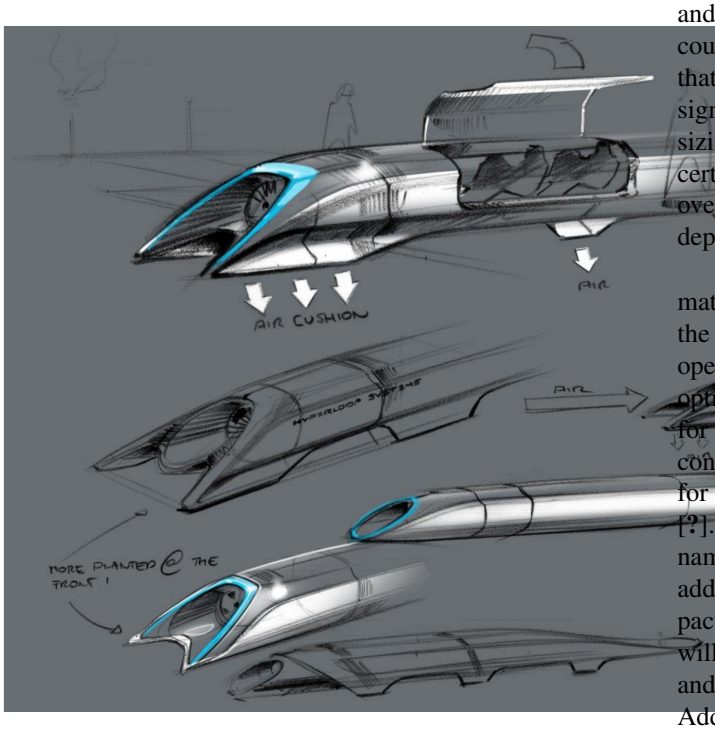

Fig. 1. Hyperloop-alpha concept sketch of the passenger pod. [?]

Although Hyperloop is similar to other vacuum tube train (VacTrain) concepts [**?**], the soft vacuum represents a distinct difference. It allows the pod to run on air-bearings, thus removing the need for a magnetic levitation system used on other VacTrain designs. The air bearings require a source of pressurized air, which is provided by a compressor powered by on-board batteries. Since Hyperloop operates at transonic speeds and a low pressure environment, the design of the pod compression system can be likened to the compressor design for aircraft turbomachinery. Furthermore, the aerodynamic concerns arising from constricted flow through a tube are prevalent in the design of inlets and nozzles on aircraft engines and the entire system faces similar weight and volume constraints. For these reasons, the modeling approach applied here is inspired heavily by methods for aircraft sizing and turbine engine cycle analysis.

Musk's original Hyperloop proposal includes individual high-level analyses of many major subsystems such as the pod compression system, elevated support structure, and propulsion system. While this demonstrates the basic viability of the concept, it does not address significant interdisciplinary couplings inherent in the Hyperloop system. These couplings introduce certain constraints that limit the degrees of freedom available in the design space. The major contribution of this work is to identify the key couplings that constrain the system and adapt aircraft sizing methods to construct a conceptual design process that accounts for them. The most significant interdisciplinary coupling arises between the passenger pod size and travel tube size. Aerodynamic concerns make it impossible to vary both pod size and tube size independently of each other. An additional less severe coupling also exists between the compression system and the thermal management system. The interdisciplinary coupling demands the use of an iterative sizing procedure that balances the various systems to provide a feasible design for any given set of design variables. The results of this sizing process show that Hyperloop remains plausible, but certain estimates from the original proposal may have been overly optimistic due to each discipline being approached independently.

The sizing process is a necessary precursor before ultimately performing a design optimization of Hyperloop with the overall objectives such as reducing construction costs, operational costs, and travel time. Performing this broader optimization is outside the scope of this work and is reserved for future investigation. The fully integrated system model is constructed using OpenMDAO, a Python-based framework for the design and optimization of highly coupled systems [**?**]. This work focuses on the aerodynamics and thermodynamics of the passenger pod itself. As such, it ignores many additional key sub-systems that will also have a large impact on the final design. A more realistic design optimization will require more detailed models of the investigated systems and additional analyses for economic and structural models. Adding all of this will result in significant growth in complexity of the Hyperloop model. OpenMDAO can provide the means to manage growing model complexity in an efficient and flexible manner. Musk's original work was released with the stated goal of jump starting a crowd sourced design effort. In that spirit, all of the analyses used in this work are released under the Apache V2.0 open source license so that they can potentially serve as a foundation for future work. Links to the source code can be found in app:Github

This paper addresses three overarching system challenges related to the passenger pod sizing. Section 2 describes the overall connectivity of the Hyperloop subsystems. Section 3 clarifies a more stringent coupling between the passenger pod and tube size and the impact this has on the passenger pod dimensions and performance. Section 4 investigates the compressor and battery requirements for the proposed Los Angeles to San Francisco route, considering the effects of maximum travel speed. Lastly, section 5 investigates the thermal equilibrium of the travel tube to provide a means of sizing the thermal management system.

2 Hyperloop Model Overview

The Hyperloop passenger pod was decomposed into five analyses that were connected to form the conceptual sizing model.

1. Compression System: Performance and power consumption of the compressors.
2. Mission Analysis: Estimate of travel time and velocity profile.

Table 1. Hyperloop passenger pod design variables

Design Variable	Value
Max. Pod Mach	0.9
Pod Bypass Mach	0.95
Compressor 1 Inlet Mach	0.6
Compressor 1 Pressure Ratio	12.47
Tube Static Pressure (Pa)	99

3. Pod Geometry: Physical dimensions of the passenger pod.
4. Tube Flow Limitations: Pod speed limitations based on choked flow restrictions.
5. Tube Wall Temperature: Equilibrium temperature of the tube.

The relationships between the systems are illustrated in Fig. 2. Feed-forward connections, or variables affecting successive subsystems, are visualized as the blue arrows in the upper-right side of the diagram. For example, the *Compressor Cycle* passes data to the *Mission Analysis*, *Pod Geometry*, and *Tube Temperature* analyses. In the lower-left side of the diagram, red arrows represent feedback connections, which establish cyclical coupling between different analyses. Table 1 summarizes the baseline values from the original proposal, which are used as design variables in this analysis. Notably, both pod radius and travel tube radius are omitted, since these variables cannot be freely varied. Instead, the assumption of a fixed area for a passenger compartment was made which, combined with the couplings shown in Fig. 2, removed these variables as design inputs. This issue is discussed in much greater detail in Section 3.

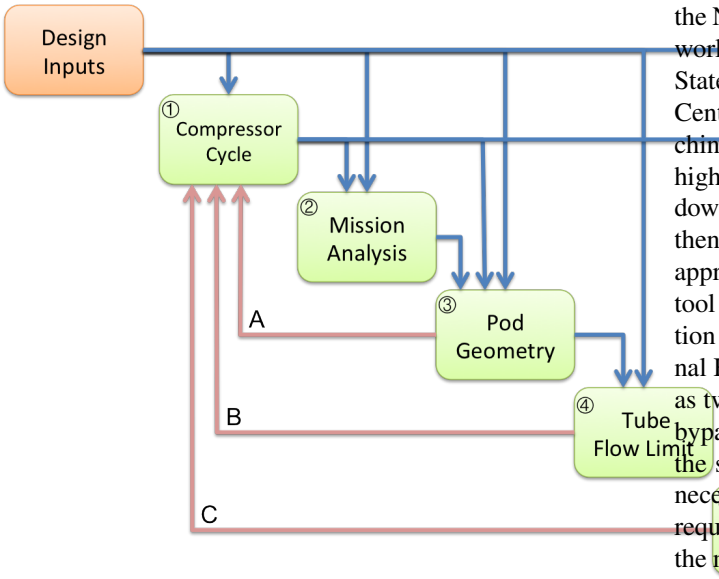

Fig. 2. Workflow and dependencies between the top-level Hyperloop assemblies.

The compression system and pod geometry analyses are each further subdivided into a number of subsystems. For this work, the pod geometry subsystem is primarily responsible for computing physical dimensions using high-level geometric relationships. Figure 3 shows the pod geometry breakdown into five further nested subsystems. This subdivision enhances modularity so that future work can replace these simple analyses with more advanced models (e.g. structural analyses and weight estimation for the various subsystems).

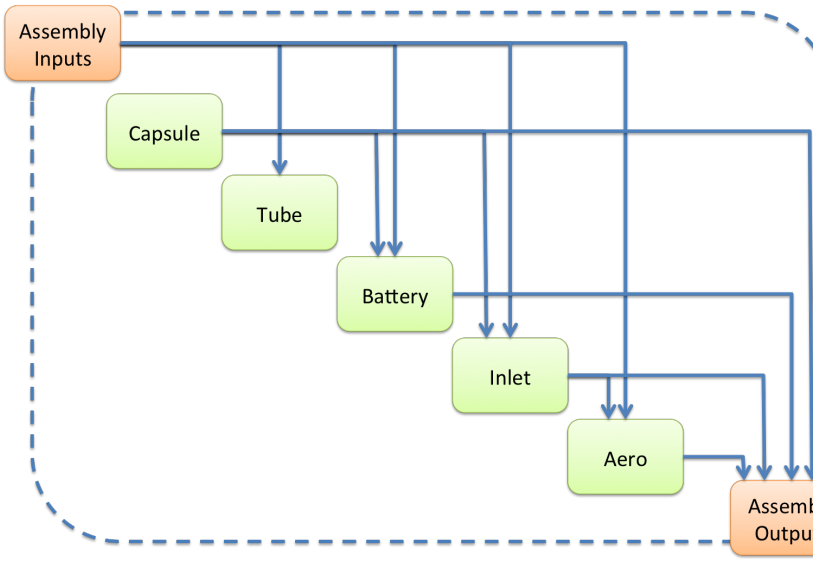

Fig. 3. Expanded pod geometry assembly

The compressor cycle performs calculations related to the thermodynamic processes of compressing, cooling, and exhausting air. The modeling approach for the compressor cycle is heavily influenced by techniques developed for the Numerical Propulsion System Simulation (NPSS) framework. NPSS was created as a joint effort between United States engine manufacturers and NASA Glenn Research Center for the purpose of simulating and analyzing turbomachinery cycles for aircraft applications [**?**]. NPSS employs a highly modular model construction where cycles get broken down into individual thermodynamic processes, which are then subsequently connected together. This object-oriented approach was followed for an open-source adaption of the tool used to predict the fluid properties and power consumption of each component in the cycle. As outlined in the original Hyperloop proposal, the compression system is modeled as two separate compressors. The first compresses the air to bypass the internal structure and passenger compartment and the second provides an additional pressure rise to reach the necessary air bearing pressure of 11 kPa. Subsequently, the required pressure ratio for the second stage is a function of the maximum pod Mach number and the first stage compressor pressure ratio. In Fig. 4 this relationship manifests as a feedback connection between the overall performance and second compressor subsystems.

Table 2. Dimensions of the passenger and cargo Hyperloop designs from the original proposal.

	Passenger	Passenger + Cargo
r_{tube}, m	1.11	1.65
A_{tube}, m^2	3.87	8.55
A_{pod}, m^2	1.4	4.0
A_{bypass}, m^2	2.47	4.55
$\frac{A_{bypass}}{A_{tube}}$	0.64	0.53
Max Mach	0.95	0.95

3 Pod and Tube Sizing

In the original Hyperloop proposal, the size of the passenger pod and the travel tube are treated as independent design variables, free to vary within reasonable ranges of each other. Two different configurations are proposed: a smaller pod for passengers and a larger pod for both passengers and cargo. The two configurations had slightly different ratios of tube area to pod area with overall dimensions summarized in Table 2.

Smaller tube sizes are preferable because they provide lower construction costs. However, the tube size is coupled to the speed of the air as it passes around a pod of a given size. To understand this coupling, consider the following simplified situation: assume that the passenger pod is sealed with a fairing instead of an inlet. Figure 5 depicts this situation with the pod traveling through a frictionless tube from right to left, at some Mach number less than 1, through a stationary mass of air. For the purposes of analysis it is more convenient to consider the air speed relative to the pod, where the pod is stationary and the air is moving from left to right with some relative Mach number, M_{pod}. As the air moves around the pod, it must fit into the smaller space available to it, A_{bypass}. This causes the air to accelerate to some higher Mach number, M_{bypass}. From isentropic flow equations, there is a relationship between M_{pod} and M_{bypass} that defines an area ratio, $\frac{A_{bypass}}{A_{tube}}$, where γ is the heat capacity ratio.

Nomenclature

$\gamma HeatCapacityRatio$

Nomenclature

MNMach Number

$$\frac{A_{bypass}}{A_{tube}} = \frac{M_{pod}}{M_{bypass}} \left(\frac{1 + \frac{\gamma-1}{2} M_{bypass}^2}{1 + \frac{\gamma-1}{2} M_{pod}^2} \right)^{\frac{\gamma+1}{2(1-\gamma)}} \quad (1)$$

Figure 6 show the effect of Eq. (1) over a range of values for M_{pod} and M_{bypass}. For all values of M_{pod}, shown as a family of curves, the minimum required $\frac{A_{bypass}}{A_{tube}}$ occurs exactly at $M_{bypass} = 1$. In other words, $M_{bypass} = 1$ will always give the smallest possible A_{bypass} (and hence A_{tube}) for a given M_{pod} and A_{pod}. Thus A_{tube} cannot be treated as an independent design variable without over-constraining the problem. If A_{tube} is forced to be smaller than this minimum value, not all the relative mass flow can pass freely around the pod. This excess flow would accumulate to the left of the pod in Fig. 5, with the pod acting like a piston: pressurizing the air in front of it.

Furthermore, Fig. 6 also shows that $\frac{A_{bypass}}{A_{tube}}$ increases with increasing M_{pod}. So the faster the pod travels, the larger A_{bypass} must become relative to the tube area, leaving less area for the pod. For $M_{pod} = 1$, $\frac{A_{bypass}}{A_{tube}}$ must equal 1 as well, forcing A_{pod} to be 0. Note that the values from Table 2 translate to area ratios around 0.6, which yields a much lower maximum pod speed of about Mach 0.3-0.4 for a pod without an inlet and compression system.

To get around this limitation, Hyperloop allows some mass flow to pass through the pod itself, thereby increasing the maximum achievable speed. This effectively splits the relative mass flow in A_{tube} into two streams, $A_{tube\ B}$ and $A_{tube\ C}$, as shown in Fig. 7. If we neglect the small thickness of the walls of the passenger pod itself and assume that $A_{tube\ C}$ is equal to the A_{pod}, then it follows that $A_{tube\ B}$ will be equal to A_{bypass}. Without any area contraction the flow in the bypass will not accelerate, staying equal to M_{pod}. The challenge is that the pod cannot be perfectly hollow. It must provide some space for the passengers to sit, causing blockage in the flow. This problem can be handled by adding a compression system to the pod that will force the air into a smaller area $A_{compressed}$, to move around the passengers. This would seem to solve all of the challenges associated with high travel speeds inside a tube discussed above and decouple $\frac{A_{bypass}}{A_{tube}}$ and M_{pod}.

However, in order to achieve reasonable efficiency from the compression system, the Mach number of the flow at the compressor face must be limited to less than about 0.65. For M_{pod} greater than 0.65, a diffuser must be added to the Hyperloop which will slow the air down before it enters the compressor. As depicted in Fig. 8, diffusing the flow requires expanding the area; $A_{diffused}$ must be greater than $A_{tube,c}$. Unfortunately this means that A_{bypass} must be smaller than $A_{tube\ B}$, and some acceleration of the flow around the pod will occur. Once again, $\frac{A_{bypass}}{A_{tube}}$ becomes coupled to M_{pod}, although thanks to the compression system this is now much less restrictive than if the pod is sealed.

Figure 9 shows the rise in achievable pod Mach number based on increasing amount of hollowness. This increase is dependent on the amount of space taken up by the pod outer structure, which is a ratio of dimensions shown in Fig. 8 as a non-dimensional "blockage factor" equal to $\frac{A_{diffused}}{A_{pod}}$. The higher the factor, the lower the blockage from the pod. For a nominal tube diameter of 4 meters, the maximum pod Mach increases from 0.66 for a closed pod (not shown) to 0.82 for a hollow pod with a blockage factor of 0.9. To a lesser extent, the max speed is also dependent on the compressor entrance Mach number. Changing the allowable compressor

entrance Mach number by ± 0.05 changes the maximum pod MN by roughly ± 0.01. Modifying the blockage factor by ± 0.05 changes the maximum pod MN by roughly ± 0.03. It should be noted that all of these trends are unaffected by the tube pressure, however, static pressure affects the compressor flow and power requirements discussed next.

Nomenclature

c1MNMach number at the front face of the first compressor

Nomenclature

BFBlockage Factor, diffused area over pod area

4 Compressor Power and Battery Sizing

The on-board compression system serves three purposes. It provides a means of increasing the maximum pod speed over a closed pod, supplies pressurized air to the air bearing system, and provides a small amount of thrust. The second function requires a minimum airflow to provide the fluid pressure necessary to support the vehicle weight. A thermodynamic analysis of the compressor system is also necessary to estimate on-board power requirements and overall heat rise of each pod. The compression cycle is comprised of an inlet, two compressors, a nozzle, and multiple ducts leading to air bearings. The design deviates from the original proposal by removing two heat exchangers for reasons explained in section 5. The system, shown previously in Fig. 4, is modeled as a one-dimensional cycle, representing components as thermodynamic processes that are subsequently chained together. Each component is responsible for calculating gas properties across its boundaries and appropriately enforcing conservation equations across the entire system.

This tool, later named "PyCycle", was built within the openMDAO framework and leverages Cantera [**?**] for thermodynamic calculations. The model predicts the instantaneous power consumption of the compressors, temperature and pressure rises, and upstream conditions necessary to supply sufficient airflow to the bearings. These power requirements are a function of the chosen geometry, creating the feedback loop B in Fig. 2. Combined with the mission profile described below, these requirements impact battery sizing.

The notional velocity profile described in the original proposal, shown by the solid line in Fig. 10, is programmatically modified based on the recomputed maximum velocity of the pod. The starting and final velocities of the mission profile are dictated by maximum allowable acceleration loads, while the highest plateau is governed by the choked flow limit. Therefore, the fastest portion of the trip, illustrated in red, is modified as the simulation runs and recomputes pod speed. Reducing the maximum speed also increases the total mission time, pushing the final mission segment out further as shown by the dashed lines. The integrated area under the curve represents the total length of the tube, which remains constant as the max speed varies. The speed constraints outlined earlier increase total mission time on the order of five minutes, however this will ultimately depend on the chosen tube diameter. Despite the increased mission time, the slower speeds would also allow for more forgiving acceleration loads around turns. Multiplying the calculated mission time by the maximum instantaneous compressor power consumption (plus a 30% safety margin) results in an overall battery storage requirement.

The necessary on-board battery energy was found to be negatively correlated to the max pod speed, as shown by the green curve in Fig. 11. The maximum instantaneous compressor requirements and total mission time are also directly overlaid in red and blue respectively. The negative slope of the green battery curve indicates that total mission time falls faster than the compressor power requirements increase. Although traveling at higher speeds draws more energy, the system is operated for a shorter period of time. At higher travel speeds, the total battery requirements start to flatten and the trend starts to reverse. The units are scaled such that the slopes of each curve can be more easily related to each other spatially. The overall reduction in battery size is on the order of 7%, if the speed is increased from Mach 0.7 to Mach 0.9, however the analysis only considers the on-board energy requirements. It does not consider the increased power necessary for the linear accelerators to drive the pod to higher speeds. Furthermore, the battery trend is highly dependent on the velocity profile and reducing time spent at max speed could result in a positive correlation between battery size and pod speed. Additional route analyses can be found in work done by Mathworks [**?**]. These estimated energy requirements are in agreement with Musk's work, and equate to roughly 4 battery packs from a Tesla Model-S. Notably, these estimates do not include considerations for battery cooling requirements or auxiliary power, and are based on the assertion that the compression cycle does not need to be cooled. The system-level thermal interactions and heat exchangers are analyzed next.

5 Heat Exchanger and Tube Thermal Analysis

As each pod passes through the tube, it adds energy to the air in the form of heat. Following the proposed frequency of launching a pod every six minutes, the continuous operating cycle could potentially heat the overall tube to excessive temperatures. To combat this effect, the original proposal recommends a heat exchanger that would be integrated into the compression system. These intercoolers would use water stored in on-board tanks to cool the air and assist secondary compression. The resulting steam could then be stored in a tank and offloaded once the pod reached its destination. However, initial calculations show that using water for cooling is not an ideal design for two reasons:

1) The flow rate of water needed to remove the heat added by the compressors is very large, and the sheer volume constraints of storing the resulting steam would outweigh the benefits.

2) The heat addition from each pod compressor cycle is

fairly low relative to other heat transfer mechanisms occurring between the Hyperloop tube and the external environment. Even without an active on-board cooling solution, the tube temperature would be dominated by other factors.

The following two sections provide additional details about the engineering models used to draw these conclusions.

5.0.1 Pod Cooling Requirements

The limits and requirements of a hypothetical on-board heat exchanger can be estimated with a straightforward energy balance. The effectiveness of a heat exchanger can be described as the ratio of actual heat transfer over the maximum possible heat transfer.

Nomenclature

QHeat flow rate (W)

$$Q_{released} = effectiveness \cdot \underbrace{(T_{hot,in} - T_{cold,in})\,[\dot{m}C_p]_{fluid}}$$

Q_{max} (2)

where Q_{max} is determined by the fluid with the lowest $\dot{m}C_p$ product, which dictates the maximum possible heat transfer. In order to satisfy the energy balance $Q_{released} = Q_{absorbed}$ the following must be true,

Nomenclature

$\dot{m}Massflowrate$

Nomenclature

TTemperature (K)

Nomenclature

$C_pHeatcapacityatconstantpressure(\mathrm{J}_{\overline{kg-K}})$

$$\underbrace{\dot{m}_{air}C_{p,air}(T_{out,air} - T_{in,air})}_{Q_{released}} = \underbrace{\dot{m}_{water}C_{p,water}(T_{out,water} - T_{in,water})}_{Q_{absorbed}} \quad (3)$$

where the T_{out} of each fluid is unknown. With assumed mass-flow rates and initial temperatures, a valid combination of T_{out}'s of each fluid can be found through solver iteration. Valid effectiveness levels for heat exchangers can be estimated based on the Effectiveness - Number of Transfer Units (NTU) method. The effectiveness for a counter flow heat exchanger with a $\frac{C_{p,min}}{C_{p,max}}$ of 0.25 was chosen with air and water as the working fluids. The following conditions satisfied an energy balance with an extremely optimistically assumed effectiveness of 0.9765, and the proposed requirement to fully cool the air back down to inlet temperatures.

Table 3. Heat Exchanger Fluid Properties

Fluid	C_p ($\frac{kJ}{kg-K}$)	T_{in} (K)	T_{out} (K)	$\dot{m}$ ($\frac{kg}{s}$)	Q ($\frac{kJ}{s}$)	Q_{max}
Air	1.006	791	300	0.49	-242	247.9
Water	4.186	288.15	416.6	0.45	242	247.9

Nomenclature

NTUNumber of Transfer Units

With a 35 minute trip, $0.45\frac{kg}{s} \cdot 60\frac{s}{min} \cdot 35min = 945kg$ of standard temperature/pressure water would need to be carried. Beyond weight concerns, the density of saturated steam at the given temperatures is on the order of 1-2$\frac{kg}{m^3}$ meaning that the resulting volume necessary for 2-4 atm steam tanks would be impractical given a cross-section smaller than $8m^2$. Depending on the tank temperature and pressure conditions, these tanks could exceed a hundred meters in length. This doesn't even account for the second stage heat exchanger, making the system nearly infeasible with water and unpressurized tanks. Various systems involving partial cooling, alternate coolants (such as liquid air), or pressurized tanks could be explored.

Further discussion of heat exchanger sizing can be found in the heat exchanger section of app:heatX. The calculations explore the possibility of multi-pass heat exchangers and the logarithmic mean temperature difference of the heat exchanger is considered. [**?**]· [**?**]

5.0.2 Equilibrium Tube Temperature

The onboard water cooling and vapor collection system as proposed in Ref. ? appears infeasible for reasons described above. Nevertheless some form of pod cabin cooling would be desired. If the tube temperature is not excessive, pod occupants could be kept comfortable with a relatively simple cabin air conditioning system. Cabin heat could be rejected from the refrigerant to the tube environs via conventional heat exchangers.

A simple quasi-steady equilibrium heat balance is performed to determine the approximate tube temperature. The analysis ignores heat transfer time lags and diurnal cycles. Heat is assumed to transfer and equilibrate rapidly between the pod compressor system, the rarified atmosphere inside the tube, the tube walls, and the outside environment. Further investigation is needed to determine the validity of this assumption. What in the real world would be a complex heat transfer problem is modeled here simplistically. This assessment is intended to estimate a conservative equilibrium tube temperature at full sun during the maximum heat of the day. An analysis of this level of fidelity is hoped to be sufficient to determine if a simple cabin air conditioning system could manage pod heating.

If the heat of the rarified atmosphere inside the tube exchanges rapidly with the tube wall, then the total temperature of the air entering the compressor inlet may be related to the tube wall temperature (T_{tube}) and the pod Mach number (M):

Nomenclature
PPressure ($\frac{N}{m^2}$)

Nomenclature
PRPressure Ratio

Nomenclature
PRPressure Ratio

Nomenclature
$\eta_{ad} Adiabatic Efficiency T_{t,inlet} = T_{tube}[1 + \frac{\gamma-1}{2}M^2]$(4)

Using additional isentropic relationships, the total temperature of the air exiting the pod nozzles may be written as a function of the compressor's pressure ratio (π_c) and adiabatic efficiency (η_c):

$$T_{t,exit} = T_{t,inlet}\left[1 + \frac{1}{\eta_c}\left[\pi_c^{\frac{\gamma-1}{\gamma}} - 1\right]\right] \quad (5)$$

The heating rate due to all of the pods operating in the tube may be estimated by

$$Q_{pods} = \dot{m} C_{p,air}(T_{t,exit} - T_{t,inlet})n \quad (6)$$

where n is the number of pods in transit, $\dot{m}$ is the airflow per compressor determined by the cycle analysis, and $C_{p,air}$ is the specific heat of air given by the relations in Ref. **?**.

The entire 300 mile length of the tube is assumed to be unshaded and exposed to sunlight. Only direct solar irradiance (G) is considered. At noon on a clear day at ground level, G may be as great as 1000 $\frac{W}{m^2}$, although it may be substantially attenuated on cloudy days. The heating rate due to solar irradiation is estimated by

$$Q_{solar} = \underbrace{(1-\rho_r)c_{solar}G}_{Solar Heat per unit Area}\ \underbrace{L_{tube}D_{o,tube}}_{Effective Area} \quad (7)$$

Nomenclature
$\rho Total, Hemispherical Reflectivity$

Nomenclature
GSolar Irradiance

Nomenclature
$c_{solar} Gross Irradiance Adjustment$

Nomenclature
LLength (m)

Nomenclature
$\varepsilon Emissivity Factor$

Nomenclature
$\sigma Stefan - Boltzmann constant(\mathrm{W}\frac{}{m-K})$

Nomenclature
$P_{rad} Radiated Power(W)$

where ρ_r is the total, hemispherical reflectivity of the tube's exterior surface, L_{tube} is the length of the tube, and $D_{o,tube}$ its outer diameter. c_{solar} is a gross adjustment factor intended to account for diffuse scattered irradiance (causing c_{solar} to increase), as well as shaded regions, non-normal incidence and other geometric peculiarities (causing c_{solar} to decrease). Added together, Q_{pods} and Q_{solar} represent the incoming heating rate on the tube. At this point an interesting observation may be made. Using representative values for each of the system parameters, it is estimated that the heat generated by the pods in transit amounts to a small fraction of the total heating rate. Insolation appears responsible for more than 95% of tube heating. The impact of solar heating, of course, may be abated by coating or shading the tube's steel surface with a highly reflective and emissive material.

On the other side of the thermal balance, radiation and convection heat transfer from the tube are assumed to be the primary heat loss mechanisms. The radiative heat transfer is estimated by

$$Q_{rad} = \underbrace{\varepsilon\sigma(T_{tube}^4 - T_{amb}^4)}_{Radiated Power per unit Area}\ \underbrace{\pi L_{tube}D_{o,tube}}_{Surface Area} \quad (8)$$

where ε is the total, hemispherical emissivity of the tube's exterior surface, σ is the Stefan-Boltzmann constant, and T_{amb} is the ambient temperature. The heat transfer surface is assumed to be gray, and the surroundings are assumed to be isothermal and black. Convection heat transfer from the tube to the surroundings is estimated using a correlation of the Nusselt number: [**?**] (Nu, defined as $\frac{hD_{o,tube}}{k}$)

Nomenclature
gAcceleration of gravity, 9.81 ($\frac{m}{s^2}$)

Nomenclature
$\beta Volume coefficient of expansion(K)$

Nomenclature
$\upsilon Kinematic Viscosity(\mathrm{m}^2\frac{}{s})$

Nomenclature
PrPrandtl Number, $\frac{\upsilon}{\alpha}$

Nomenclature
GrGrashof Number, $\frac{g\beta\delta TL^3}{\nu^2}$

Nomenclature
RaRayleigh Number, $\frac{\rho U_\infty L}{\mu}$

Nomenclature
NuNusselt Number, $\frac{hL}{k}$

Nomenclature
hHeat transfer coefficient ($\frac{W}{m^2-K}$)

Nomenclature
kThermal Conductivity ($\frac{W}{m-K}$)

$$Nu = \left(0.6 + \frac{0.387Ra^{\frac{1}{6}}}{\left[1+\left(\frac{0.559}{Pr}\right)^{\frac{9}{16}}\right]^{\frac{8}{27}}}\right)^2 \quad (9)$$

where Ra is the Rayleigh number ($\frac{g\beta}{\upsilon\alpha}[T_{tube} - T_{amb}]D^3_{o,tube}$) and Pr is the Prandtl number ($\frac{\nu}{\alpha}$). The correlation is applicable for estimating free convection from long, horizontal cylinders. Properties for air (h, k, β, ν and α) are based on the film temperature of the thermal boundary layer and are given by the regressions in Ref. ?. With the heat transfer coefficient h known from the Nusselt number, the heat lost to free convection (Q_{conv}) may be estimated from the total tube surface area.

$$Q_{conv} = \underbrace{\frac{k \cdot Nu}{D_{o,tube}}}$$

$$\underbrace{h\pi L_{tube} D_{o,tube}}_{Area}\underbrace{(T_{tube} - T_{amb})}\Delta T \quad (10)$$

The equilibrium tube temperature is determined by varying T_{tube} until the criterion $Q_{pods} + Q_{solar} = Q_{rad} + Q_{conv}$ is satisfied. Estimating a single deterministic tube temperature, however, is insufficient. The parameters of the problem have a strong influence over the resulting equilibrium temperature. For example, ambient temperature will vary substantially. A breeze can amplify convection rates by a factor of two or three, and furthermore, it is not clear what surface properties the tube may have. For these kinds of reasons, several parameters in the problem are set to vary in a Monte Carlo probability experiment. The deterministic tube temperature model above is transformed into a stochastic model by replacing portions of its input with continuous random values. The random values are derived from probability distributions around the model's nominal values as listed in Table 4.

Table 4. Uncertainty variables used in the Monte Carlo experiment.

1,0l c c c c c

Variable	Mode	Model	Min	Max	Std. Dev
T_{amb}	305 K	Normal	-	-	4.5 K
G	$1000\frac{W}{m^2}$	Triangular	$200\frac{W}{m^2}$	$1000\frac{W}{m^2}$	-
ρ	0.5	Triangular	0.4	0.9	-
ε	0.5	Triangular	0.4	0.9	-
η_c	0.69	Triangular	0.6	0.8	-
n	34	Triangular	-	-	2
c_{solar}	0.7	Triangular	0.5	1.0	-
c_{conv}	1.0	Triangular	0.9	3.0	-

A histogram and a normal distribution of tube temperature based on 15,000 samples are shown in Fig. 12. The mean tube temperature is 108 F with a standard deviation of 11 F. Exceeding 137 F only occurs in 0.5% of the possible scenarios generated. This Monte Carlo assumes a fixed tube diameter of 4 meters, for reasons outlined in Section 3. Repeating the experiment closer to the original 2 meter diameter results in a distribution with approximately the same mean and a lower standard deviation of 9.7 F.

The sub-iteration of the thermal discipline then feeds back into the overall Hyperloop convergence loop, both affected by and contributing to the compression cycle, creating feedback C in Fig. 2. The analysis suggests that the dominant heating factors are a direct result of the massive tube structure, with only 5% of the heat contributed from the pods. The thermal management should therefore be incorporated into the tube design, rather than integrated into the volume and weight constrained pod design. Considerations for solar panel shielding as outlined in the original proposal would produce even more thermally optimistic results.

6 Conclusions

Using openMDAO and pyCycle, a publicly extensible model of the Hyperloop concept was created to investigate the features and assertions of the original design. The refined analysis illuminates several interdisciplinary couplings that alter two major aspects of the initial concept. First, the pod travel speed and the tube cross sectional area are linked, forcing the tube size to be to be roughly twice the diameter of the original specification, in order for the pod to reach Mach 0.8. Second, the steady-state tube temperature is dominated by ambient thermal interactions unrelated to the heat generated by the pod compression system. As a result, the two water-based heat exchangers originally prescribed for thermal management are eliminated. Although this work iden-

tifies some necessary refinements to the Hyperloop design, the core concept remains potentially feasible and warrants continued investigation. This work emphasizes the importance of maintaining a systems-level approach and provides toolsets capable of managing the growing complexity. The modeling platform is intended to serve as an easily accessible baseline that is straightforward to expand and delve deeper into this unique multidisciplinary endeavor.

Acknowledgements

ASME Technical Publications provided the format specifications for the Journal of Mechanical Design, though they are not easy to reproduce. It is their commitment to ensuring quality figures in every issue of JMD that motivates this effort to have authors review the presentation of their figures.

Thanks go to D. E. Knuth and L. Lamport for developing the wonderful word processing software packages TEX and LATEX. We would like to thank Ken Sprott, Kirk van Katwyk, and Matt Campbell for fixing bugs in the ASME style file `asme2ej.cls`, and Geoff Shiflett for creating ASME bibliography stype file `asmems4.bst`.

References

Appendix A: Head of First Appendix

Avoid Appendices if possible.

Appendix B: Head of Second Appendix

Subsection head in appendix

The equation counter is not reset in an appendix and the numbers will follow one continual sequence from the beginning of the article to the very end as shown in the following example.

$$a = b + c. \tag{11}$$

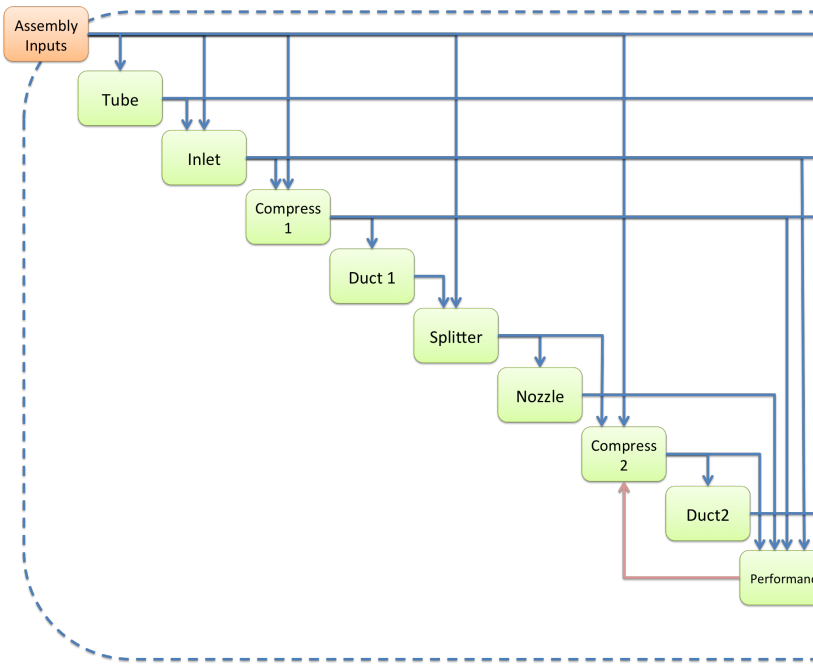

Fig. 4. Expanded compressor cycle assembly

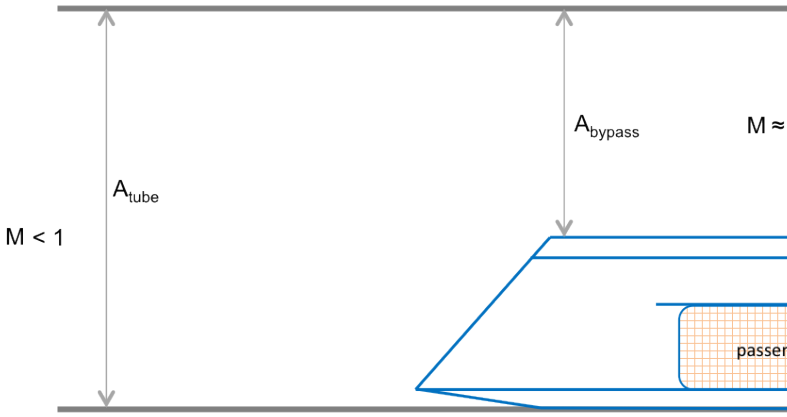

Fig. 5. Longitudinal view of a passenger pod with no inlet and no compression system.

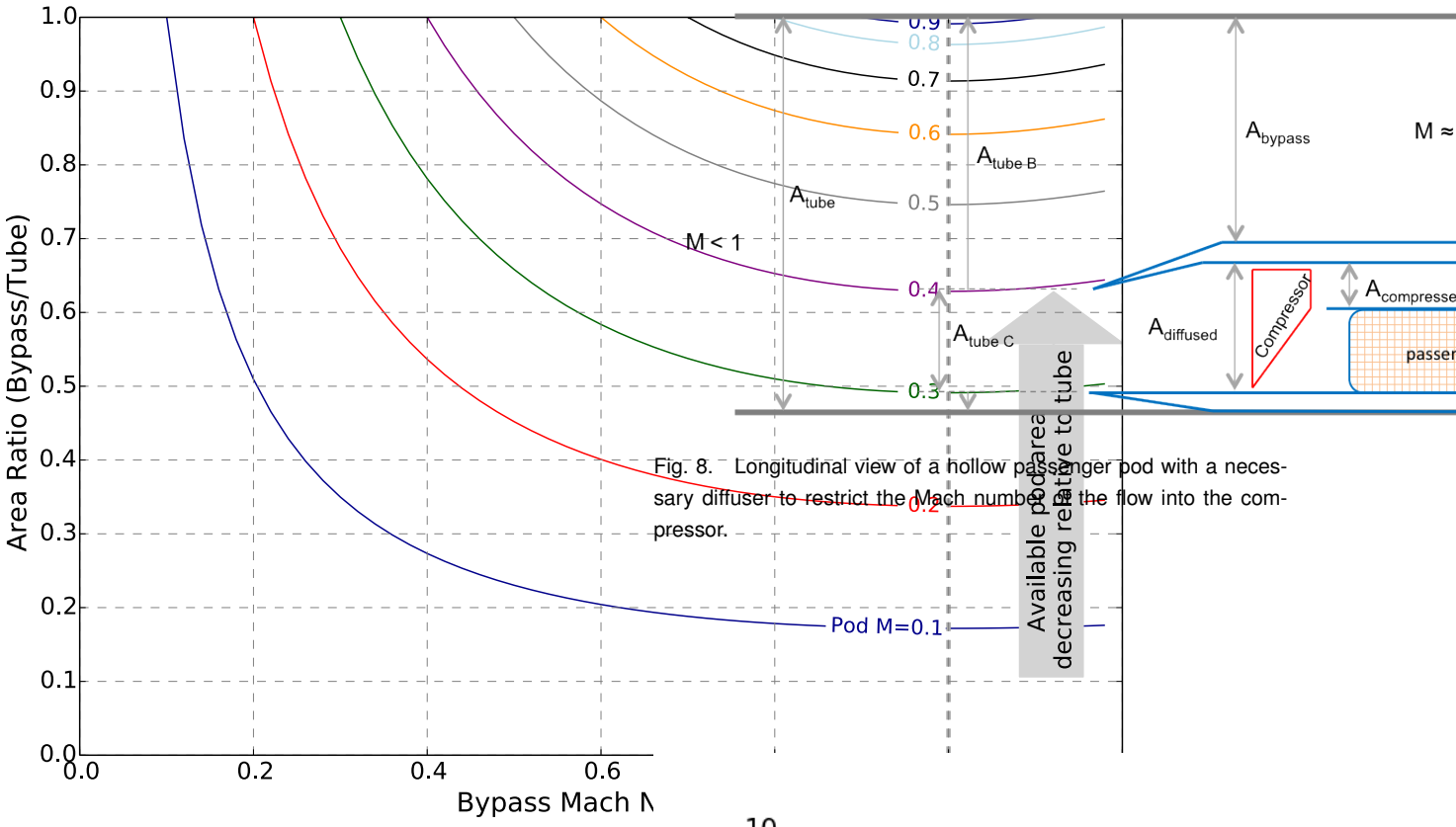

Fig. 8. Longitudinal view of a hollow passenger pod with a necessary diffuser to restrict the Mach number of the flow into the compressor.

Fig. 6. The required area ratio reaches a minimum value at $M_{bypass} = 1$ for all values of M_{pod}, given the closed pod configuration illustrated in Figure 5.

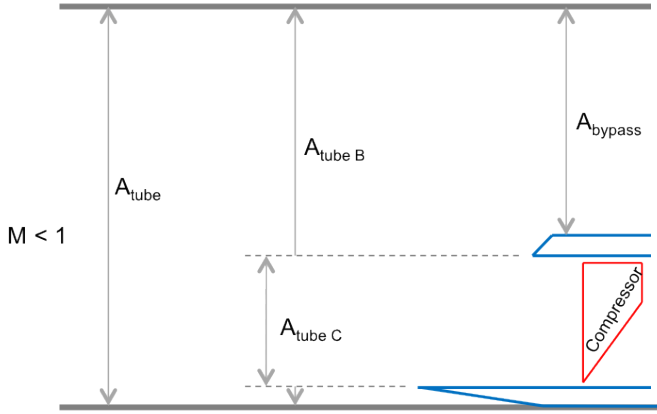

Fig. 7. Longitudinal view of a hollow passenger pod that lets mass flow pass through it.

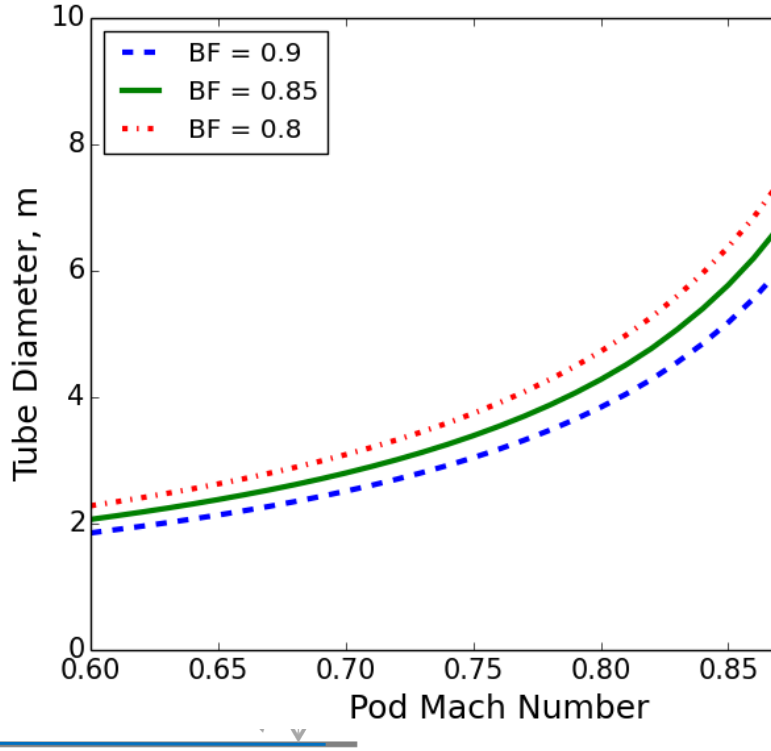

Fig. 9. Exponential relationship between pod speed and required tube diameter, for three blockage factors $\frac{A_{diffused}}{A_{pod}}$.

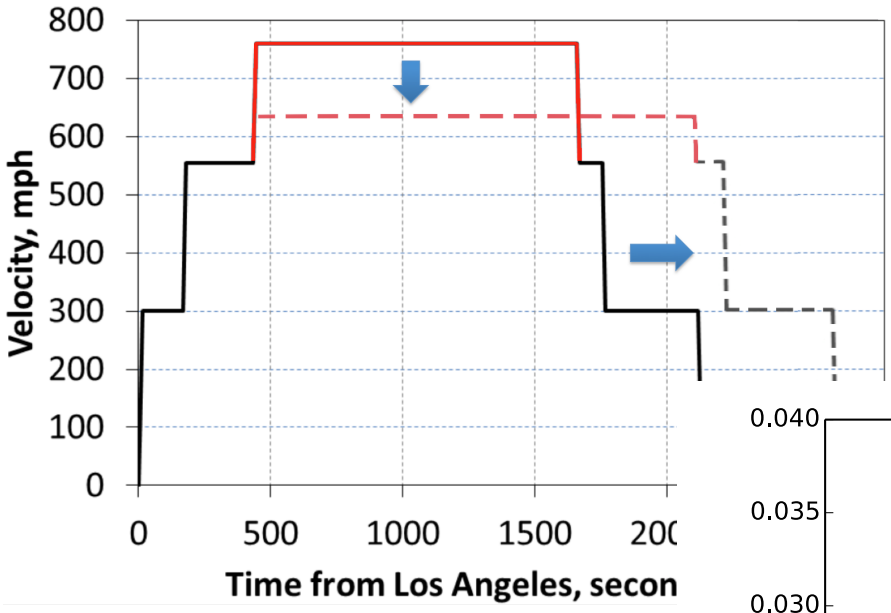

Fig. 10. Velocity profile described in the original proposal, with the programmatically modified section highlighted in red.

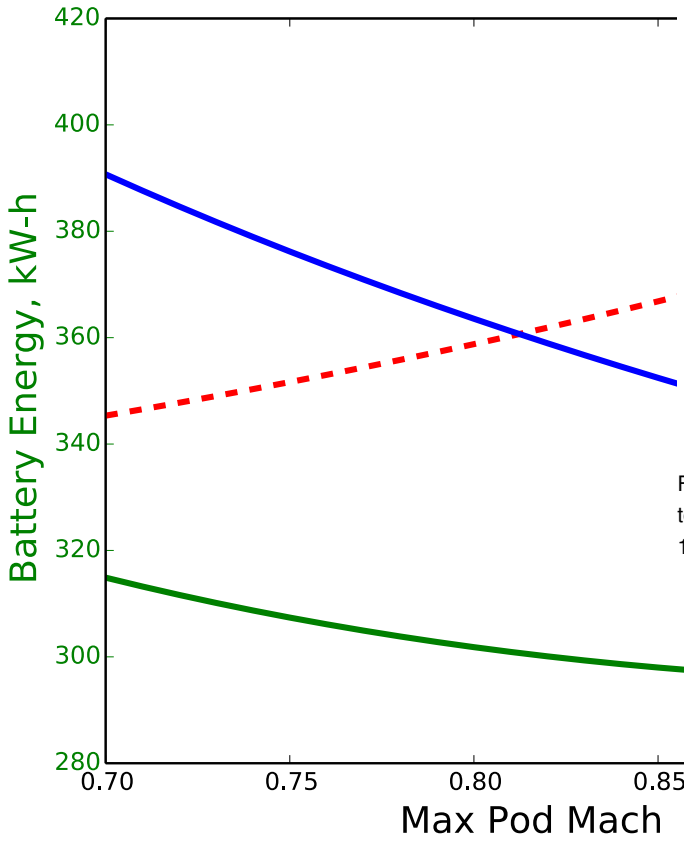

Fig. 11. Battery requirements, compressor power, and mission time as a function of pod speed.

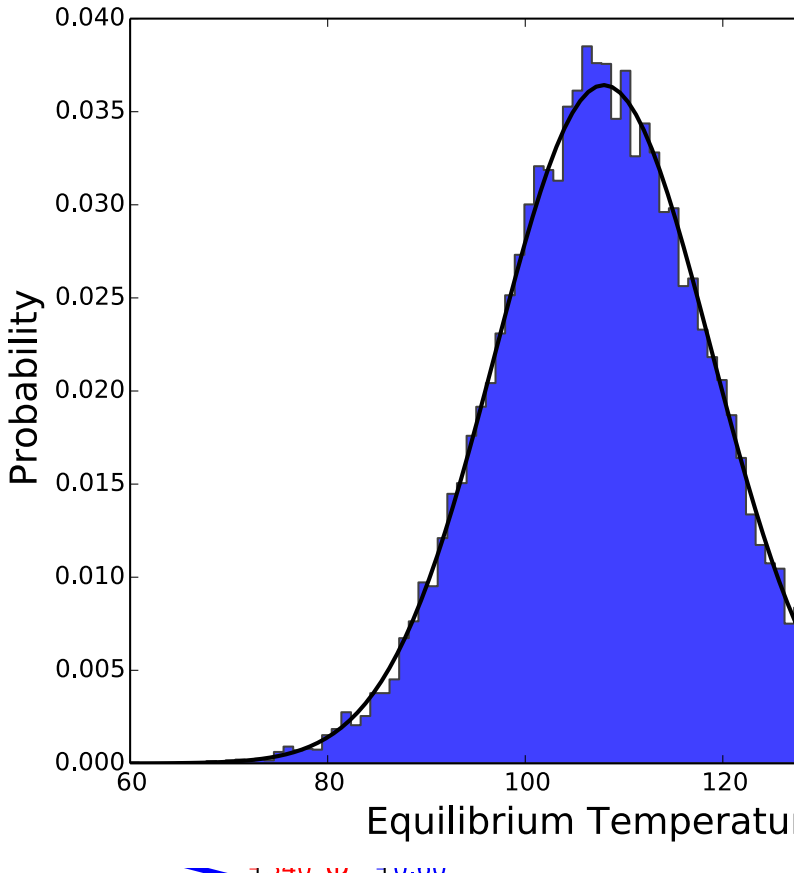

Fig. 12. Monte Carlo uncertainty analysis of the equilibrium tube temperature. Histograms and normal distribution generated from 15,000 samples using a bin span of 1°.